



Effect of scratch on corrosion resistance of calcium phosphate conversion coated AZ80 magnesium alloy

Xue-jiao JIA¹, Jiang-feng SONG^{1,2}, Xiao-rong QU³, Fu-yong CAO⁴, Bin JIANG^{1,2}, Andrej ATRENS⁵, Fu-sheng PAN^{1,2}

1. State Key Laboratory of Mechanical Transmissions, Chongqing University, Chongqing 400044, China;

2. National Engineering Research Center for Magnesium Alloy, Chongqing University, Chongqing 400044, China;

3. Qinghai Salt Lake Industry Co., Ltd., Qinghai 816000, China;

4. Center for Marine Materials Corrosion and Protection, College of Materials, Xiamen University, Xiamen 361005, China;

5. School of Mechanical and Mining Engineering, The University of Queensland, Brisbane Qld 4072, Australia

Received 12 January 2021; accepted 24 August 2021

Abstract: In order to analyze the effect of scratch on the corrosion behaviour of a calcium phosphate conversion coating (CPCC) on AZ80, the electrochemical testing, scanning vibrating electrode technique (SVET), immersion test and hydrogen evolution experiment were performed to study the corrosion resistance of AZ80, AZ80 with CPCC and coated AZ80 with scratch. The results show that the coating improves the corrosion resistance of the AZ80 from a current density of (85 ± 4) to (4 ± 1) $\mu\text{A}/\text{cm}^2$. When the coating was damaged, its protection on substrate would be reduced. The scratch with a length of around 12 mm on the coating reduced the corrosion resistance to a current density of (39 ± 1) $\mu\text{A}/\text{cm}^2$. In addition, the corrosion occurred initially in the scratch area and the corrosion site first occurred at the junction of the scratch and the coating. Besides, the micro corrosion mechanism of the specimen containing scratch was clarified.

Key words: magnesium alloy; AZ80 alloy; scratch; conversion coating; corrosion resistance; scanning vibrating electrode technique (SVET)

1 Introduction

Magnesium alloys exhibit low density, high specific strength, high thermal conductivity, high electromagnetic properties, high castability and good recyclability, and have been widely used in the electronics, aerospace and automotive industries [1–5]. For example, magnesium alloys were used in the steering wheels, central control boards and wheel hubs in automotive construction due to their great lightweighting potential [6,7]. Among these magnesium alloy automotive parts, wheel hub is the under spring parts and thus shows the greatest lightweighting potential. Past research

indicated that reducing the mass of the wheel hub is 8–10 times more effective in lightweighting than reducing the mass of body parts. As a result, investigations on magnesium alloy wheel hubs to replace steel wheel hubs or aluminum alloy wheel hubs have attracted much attention.

AZ80 magnesium alloy has been generally used to manufacture wheel hubs due to its high comprehensive mechanical properties, high forgeability and moderate corrosion resistance [8]. Generally, surface treatment has been applied on the magnesium alloy wheel hub to further enhance its corrosion resistance.

Over the past decades, the chemical conversion coatings [9], electroplating/electroless

plating [10–12], anodic oxidation [13], plasma electrolytic oxidation [14–16] and composite multi-layer coatings [13,17] have been developed to improve the corrosion resistance of magnesium alloys. Chemical conversion coatings on magnesium alloys such as phosphate, stannate, vanadate, rare earth salt and hydrotalcites coating systems have been proposed [18–21]. Among them, calcium phosphate conversion coating (CPCC) has attracted much attention due to the low-cost, simplicity in operation, environment-friendliness and stability in neutral pH solution [22,23]. Moreover, CPCC has been widely used on magnesium alloy parts such as steering wheel, central control board, door inner, car seat frame, transfer case and instrument panel.

During automobile service, scratches and other defects are inevitably generated by stones or other objects on the surface of magnesium alloy wheel hub. Understanding the effect of scratches and other defects on the corrosion behaviour of the coating is of great importance for the industrialization of the chemical conversion coating. However, so far, few investigations have paid attention to the effect of the scratch on the corrosion resistance of the calcium phosphate conversion coated AZ80 magnesium alloy. The mechanism of corrosion initiation and expansion of the conversion coating with scratch are not clear.

In order to promote the industrialization of the calcium phosphate conversion coating, a scratch was designed on the CPCC to simulate the possible defects generated from the practical usage of the coating. In this study, the effect of a scratch on the corrosion behaviour of the CPCC on AZ80 was investigated. For comparison, the corrosion behaviours of AZ80 and AZ80 with CPCC were also investigated. The corrosion mechanism of the CPCC with a scratch was clarified by electrochemical impedance spectroscopy (EIS), potentiodynamic polarization analysis, scanning vibrating electrode technique (SVET) and immersion test.

2 Experimental

2.1 Materials

Forged magnesium alloy AZ80 specimens with dimensions of 20 mm × 20 mm × 3 mm were bought from Yueyang Yuhua Metallurgical New

Materials Co., Ltd. The chemical composition is shown in Table 1. AZ80 specimens were ground with different grades of SiC sandpaper (400[#], 800[#], 1000[#] to 1500[#]), cleaned with deionized water, rinsed with alcohol, and dried immediately in air.

Table 1 Chemical composition of AZ80 magnesium alloy (wt.%)

Al	Zn	Mn	Si	Fe	Mg
8.500	0.549	0.181	0.005	0.002	Bal.

2.2 Preparation of CPCC and scratch

AZ80 with CPCC specimens were prepared by immersing in the phosphate solution at room temperature for 1 min, cleaned with deionized water and dried in air. The phosphate solution was provided by a local manufacturer of magnesium alloy automotive parts named BoAo Magnesium Aluminum Co., Ltd. The solution was composed of 1.3 g/L CaO, 23.3 mL/L H₃PO₄, 14.4 mL/L HNO₃ and 12.6 mL/L CH₃COOH. The pH value of the phosphate solution was adjusted to 2–3 with deionized water.

The scratch with a width of around 200 μm and a length of about 12 mm was prepared artificially on the CPCC using a needle. The depth of the scratch was designed to penetrate down to the substrate.

The AZ80 specimen without any treatment, AZ80 coated with CPCC and the coated AZ80 with a scratch were designated as AZ80, CPCC and CPCC with scratch, respectively.

2.3 Specimen characterization

The microstructures of AZ80 and CPCC were characterized using scanning electron microscope (SEM, JSM–7800F, JEOL, Japan). The phase constituents of AZ80 and CPCC were studied using energy dispersive spectroscopy (EDS, Inca Energy 350 Oxford, UK), X-ray photoelectron spectroscopy (XPS, ESCALAB 250Xi Thermo Scientific, USA) and X-ray diffractometer (XRD, RIGAKU, Japan). The XPS was carried out on the surface of CPCC using Al K_α radiation (1486.6 eV) with a pass energy of 30 eV. The corresponding peaks were analyzed by using the software Avantage. The XRD was performed on AZ80 and CPCC using Cu radiation (λ=0.154 nm) operated at 40 kV and 15 mA with a glancing angle of 1.5°. The cross section of CPCC specimen was

investigated by SEM and the thickness of the coating was identified.

2.4 Electrochemical testing

An electrochemical workstation (chi660e, China) was used to analyze the corrosion behaviour of the specimens in a 3.5 wt.% NaCl solution at 25 °C. A three-electrode system with a platinum plate as the counter electrode, the specimen as the working electrode (exposing area of 1 cm²), and the saturated calomel reference electrode (SCE) as the reference electrode was used. For the scratched specimen, the scratch on the specimen for electrochemical test was also prepared artificially using a needle, just like other experimental specimens. The scratched specimen was then connected in the electrochemical cell, and the scratched area should be immersed in the corrosive solution. All the specimens were immersed in the 3.5 wt.% NaCl solution for 15 min before electrochemical testing, and then exposed in the solution for the open circuit potential (OCP) test to ensure that the system was in a steady state. The electrochemical impedance spectra (EIS) were measured using a disturbing potential of 10 mV and performed from 10 kHz to 10 mHz at OCP. The EIS data were fitted by ZSimpWin software with proper equivalent circuits. The potentiodynamic polarization curves of all the specimens were measured at a scanning rate of 0.1 mV/s in a potential range for ±300 mV (vs SCE) from the OCP. Three parallel specimens for each condition were used to ensure the reproducibility.

The scanning vibrating electrode technique (SVET) was carried out on CPCC with scratch specimens with Bio-Logic Uniscan M470 at room temperature. Specimens after immersion in the NaCl solution for 15 min, 1 h, 3 h and 6 h were scanned by SVET, respectively. The vibrating microprobe vibrated at 80 Hz at an average distance of 200 μm from the surface of the specimen with an amplitude of 30 μm. Each scan was composed of 25 × 30 points and took about 15 min.

2.5 Immersion test

AZ80, CPCC and CPCC with scratch specimens were immersed in 500 mL 3.5 wt.% NaCl solution in closed containers for 72 h at room temperature. The morphology changes were recorded by camera at different time. The evolution

of the surface morphologies and compositions of CPCC and CPCC with scratch specimens after immersion for different time were also studied by SEM and EDS.

The corrosion resistances of the specimens were also characterized by hydrogen evolution test in 3.5 wt.% NaCl solution at 25 °C for 132 h [24]. Specimens with exposed areas of 4 cm² were placed under an inverted funnel with a graduated burette connected. The amount of hydrogen evolved from each specimen was recorded intermittently during the 132 h immersion. Three parallel specimens were used for better accuracy. The hydrogen evolution rate v_{HER} can be shown as [25,26]

$$v_{\text{HER}} = V/(st) \quad (1)$$

where V is the volume of hydrogen evolution (mL), s is the exposure area, and t is the immersion time.

3 Results and discussion

3.1 Characteristics of AZ80 and CPCC

Figure 1 displays the SEM images, EDS and XRD analyses of AZ80 and CPCC. The second phase in AZ80 magnesium was identified as Mg₁₇Al₁₂ (Fig. 1(f)). It is reported that the second phase will induce galvanic corrosion, resulting in poor corrosion resistance of the AZ80 magnesium alloy [26–28]. The CPCC on AZ80 exhibited a micro-cracked structure (Fig. 1(c)) with a thickness of about 800 nm (Fig. 1(e)). The microcracks are common on the surface of chemical conversion coated magnesium alloys [29,30]. The formation of micro-cracks is likely owing to the reduced molar volume of the conversion coating from dehydration process [31]. The entrapped hydrogen-induced coating cracking mechanism could also lead to the formation of cracks [32]. The EDS results (Fig. 1(d)) of CPCC showed that CPCC was composed of Mg (69.9%), Al (12.4%), O (10.7%), P (3.7%) and Ca (3.3%). The molar ratio of Ca to P was about 1.0, which was close to that of dicalcium phosphate dihydrate (DCPD). The XRD results (Fig. 1(f)) revealed that the main component of CPCC was DCPD, which was consistent with the EDS results.

The chemical states of the surface elements on the CPCC were measured using XPS. The XPS survey spectra contained peaks of O, P, Ca, Mg, Al and C (Fig. 2(a)), and the element contents are shown in Table 2. The C peak is commonly seen

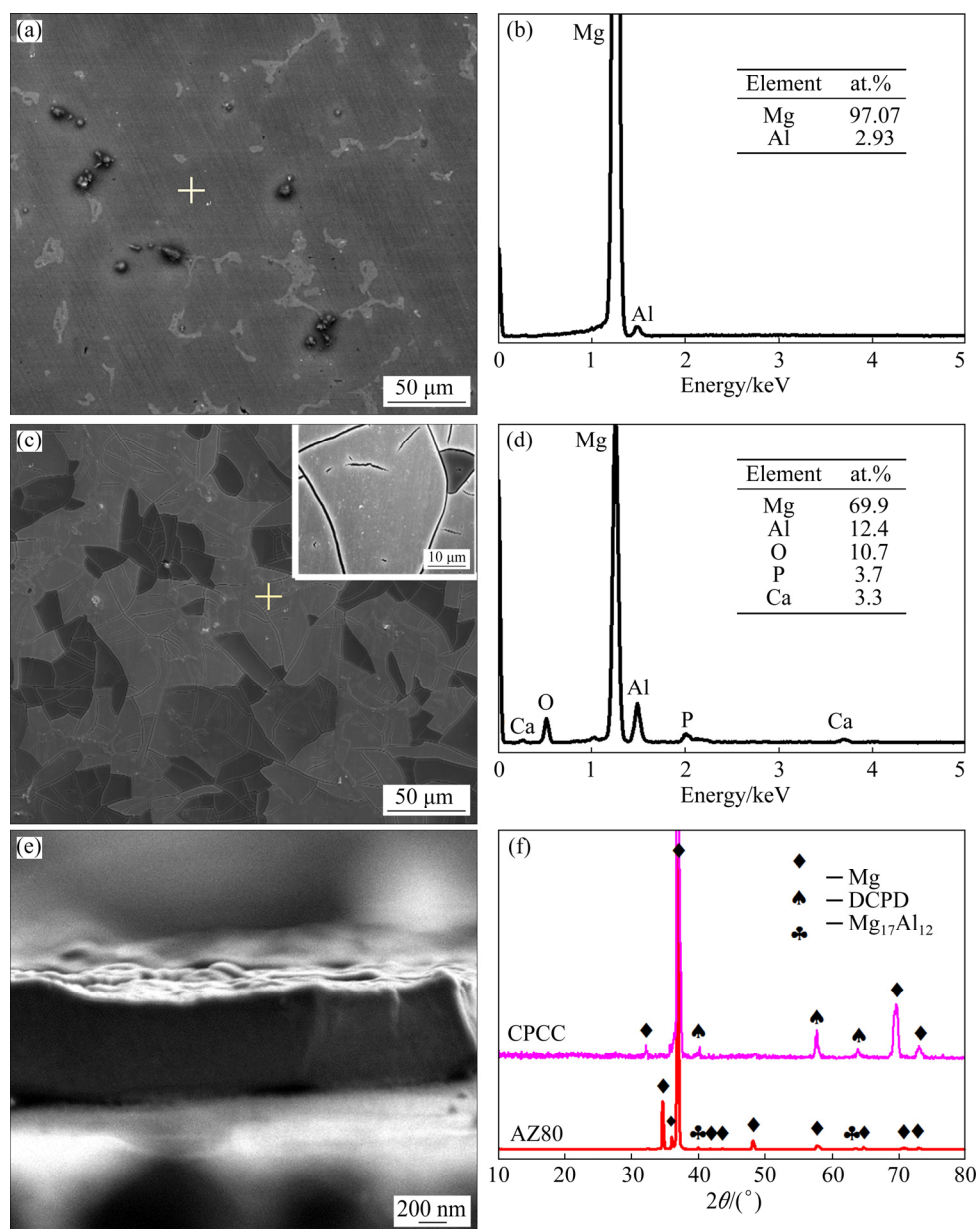


Fig. 1 SEM images and EDS analyses of AZ80 (a, b), CPCC (c, d), cross-section image of CPCC (e), and XRD patterns of AZ80 and CPCC (f)

in XPS results because of the extraneous hydrocarbons in the environment [22]. The Mg and Al peaks were from the AZ80 substrate because the CPCC was thin with a micro-cracked structure. The peaks of O, P, Ca reflected the composition of CPCC. The high-resolution XPS spectra of the Ca 2p, P 2p and O 1s are depicted in Figs. 2(b)–(d), respectively. Two prominent peaks of Ca 2p_{3/2} (347.3 eV) and Ca 2p_{1/2} (350.9 eV) were detected, which were generally assigned to the Ca—P compound [33–35]. The P 2p at binding energy of 133.7 eV was attributed to the HPO₄²⁻ radical of CaHPO₄ [36]. The high-resolution O 1s showed two

peaks at 531.3 and 533.0 eV, which were related to the P—O and P—O—P, respectively [34]. This kind of O in single bond with P (P—O) forms a chelating bridge with Mg and even Ca atoms to create a compacted bonded film [37]. Hence, the XPS results confirmed that CPCC was composed of DCPD.

3.2 Corrosion behaviour

3.2.1 Electrochemical analysis

In order to evaluate the corrosion resistance of CPCC and the effect of a scratch on the corrosion resistance of CPCC, the electrochemical properties

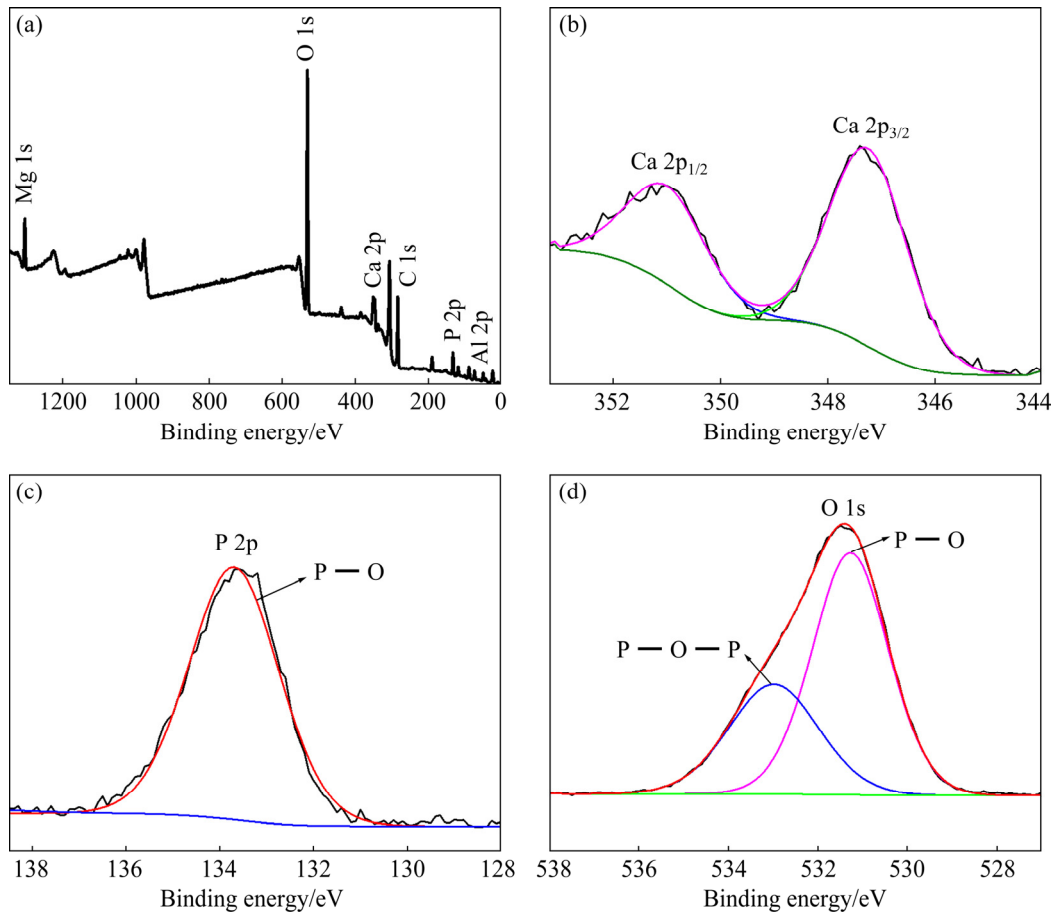


Fig. 2 XPS spectra of CPCC: (a) Survey scanning spectrum; (b) High-resolution spectrum of Ca 2p; (c) High-resolution spectrum of P 2p; (d) High-resolution spectrum of O 1s

Table 2 Element contents of CPCC measured by XPS (at.%)

O 1s	C 1s	P 2p	Al 2p	Ca 2p	Mg 1s
45.7	31.8	6.5	6.3	5.0	4.7

of AZ80, CPCC and CPCC with scratch were assessed using potentiodynamic polarization and EIS.

Figure 3 and Table 3 show the potentiodynamic polarization curves of all specimens after immersion in 3.5 wt.% NaCl solution. The results show that the corrosion current density of CPCC ($(4\pm 1) \mu\text{A}/\text{cm}^2$) was over an order of magnitude lower than that of AZ80 ($(85\pm 4) \mu\text{A}/\text{cm}^2$), demonstrating that CPCC improved the corrosion resistance of AZ80. When the CPCC was damaged to a certain extent, the current density (J_{corr}) of the CPCC with scratch increased to $(39\pm 1) \mu\text{A}/\text{cm}^2$ from $(4\pm 1) \mu\text{A}/\text{cm}^2$ for CPCC. The increased corrosion rate was attributed to the scratch of the coating shortening the mass

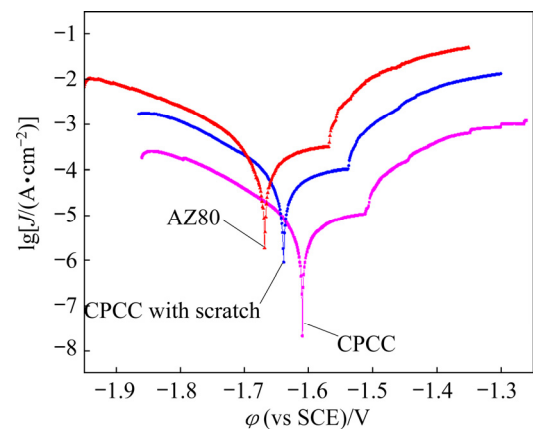


Fig. 3 Potentiodynamic polarization curves of AZ80, CPCC and CPCC with scratch measured in 3.5 wt.% NaCl solution

transfer channel of the corrosion process, so that the solution directly reached the substrate. However, the corrosion current density of scratched coating was still lower than that of AZ80, indicating that the damaged coating still has a protective effect on the magnesium alloy.

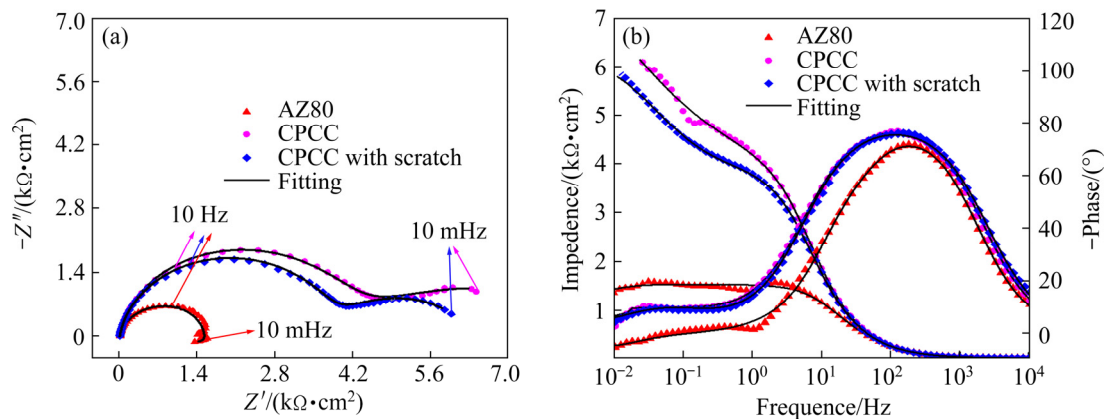
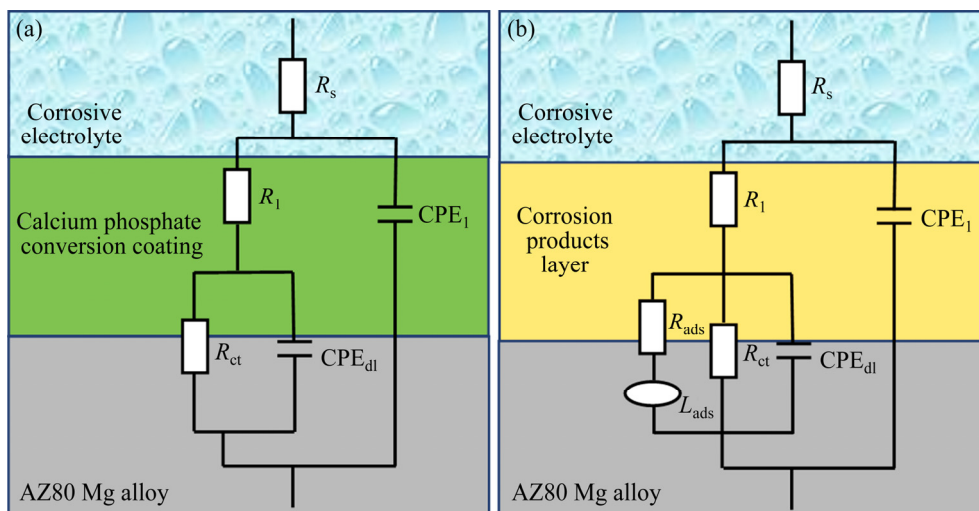
Table 3 Corrosion parameters of AZ80, CPCC and CPCC with scratch

Specimen	φ_{corr} (vs SCE)/V	J_{corr} /($\mu\text{A}\cdot\text{cm}^{-2}$)
AZ80	-1.67 ± 0.25	85 ± 4
CPCC	-1.61 ± 0.12	4 ± 1
CPCC with scratch	-1.64 ± 0.15	39 ± 1

EIS can effectively reflect the corrosion performance of the specimens. Nyquist diagrams of AZ80, CPCC and CPCC with scratch measured in 3.5 wt.% NaCl solution are presented in Fig. 4(a) and Bode diagrams are presented in Fig. 4(b). The overall corrosion resistance of the specimens can be evaluated by the impedance modulus at low-frequency and the radius of the Nyquist curves. In general, the higher the impedance modulus, the larger the radius of the Nyquist curves, and the better the corrosion resistance [38–40]. Therefore, the corrosion resistance order of the specimens is:

CPCC > CPCC with scratch > AZ80, which is consistent with the potentiodynamic polarization results.

The equivalent circuit diagrams for EIS of AZ80, CPCC and CPCC with scratch are presented in Fig. 5. In the equivalent circuits, R_s corresponds to the electrolyte solution resistance. As for CPCC and CPCC with scratch specimens, R_1 describes the phosphate conversion coating resistance, R_{ct} represents the charge transfer resistance, CPE_1 corresponds to the constant phase element of the coating, and CPE_{dl} represents the double-layer constant phase element. For AZ80 specimens, R_1 and CPE_1 correspond to the loose corrosion products layer resistance and constant phase element, respectively; R_{ct} and CPE_{dl} represent the charge transfer resistance and the double-layer constant phase element, respectively; R_{ads} and L_{ads} represent the low frequency (LF) inductive loop. The EIS spectra (Fig. 4) of CPCC and CPCC with

**Fig. 4** Nyquist diagram (a) and Bode diagram (b) of AZ80, CPCC and CPCC with scratch measured in 3.5 wt.% NaCl solution**Fig. 5** Equivalent circuit diagrams for CPCC and CPCC with scratch (a) and AZ80 (b)

scratch consisted of two capacitive loops at high frequency (HF) and middle frequency (MF). The equivalent circuit diagram of CPCC and CPCC with scratch is presented in Fig. 5(a). Generally, the capacitive loops at HF and MF reflect the physicochemical process of the coating and their specific structural features or electrochemical properties [31,41,42]. The EIS of AZ80 immersed in NaCl solution consisted of two capacitive loops at HF and MF and an inductive loop at low frequencies (LF), which is consistent with the equivalent circuit shown in Fig. 5(b). The additional inductive loop for AZ80 is attributed to the adsorption and desorption of the corrosion products such as $Mg(OH)_2$, demonstrating the formation of a thin film of $Mg(OH)_2$ during the period for building a stable OCP in 3.5 wt.% NaCl solution before EIS test. The formation of $Mg(OH)_2$ indicates slow corrosion reaction on the surface of AZ80 [43–45].

The fitting results are listed in Table 4, and the fitting quality was evaluated by chi-square (χ^2) error value. In CPCC and CPCC with scratch, Y_1 is the

conductance of phosphate conversion coating, and in AZ80, Y_1 is the conductance of the corrosion products layer; Y_{dl} is the double-layer conductance; n_1 and n_{dl} are the angular frequency. Generally, the corrosion resistance can be assessed by the values of R_1 and R_{ct} . The values of R_1 and R_{ct} of CPCC were about 4 times those of AZ80, which indicates that CPCC improves the corrosion resistance of AZ80. Furthermore, the R_1 and R_{ct} values of the scratched CPCC were a bit lower than those of the CPCC, indicating that the corrosion resistance of CPCC after scratching was slightly decreased.

3.2.2 Corrosion morphologies

The corrosion morphologies of the specimens immersed in 3.5 wt.% NaCl solution for different time are shown in Fig. 6. After immersing for 3 h, there was obvious localized corrosion on the surface of AZ80, which is attributed to the microgalvanic acceleration of the corrosion of the matrix phase by the adjacent second phase particle. As the immersion time increased, the corrosion proceeded more deeply. After 48 h immersion, the

Table 4 Fitted parameters for EIS spectra depicted in Fig. 4

Specimen	$R_s/(\Omega \cdot \text{cm}^2)$	$R_1/(\Omega \cdot \text{cm}^2)$	CPE_1		$R_{ct}/(\Omega \cdot \text{cm}^2)$	CPE_{dl}		χ^2
			$Y_1/(\Omega^{-1} \cdot \text{cm}^{-2} \cdot \text{s}^n)$	n_1		$Y_{dl}/(\Omega^{-1} \cdot \text{cm}^{-2} \cdot \text{s}^n)$	n_{dl}	
AZ80	18.36	1.133×10^3	9.005×10^{-6}	0.9412	1.232×10^3	2.582×10^{-5}	1.0000	4.043×10^{-3}
CPCC	15.98	4.055×10^3	9.656×10^{-6}	0.9249	4.978×10^3	7.144×10^{-4}	0.4966	9.083×10^{-4}
CPCC with scratch	14.10	3.887×10^3	1.074×10^{-5}	0.9140	2.468×10^3	1.160×10^{-4}	0.7110	5.981×10^{-3}

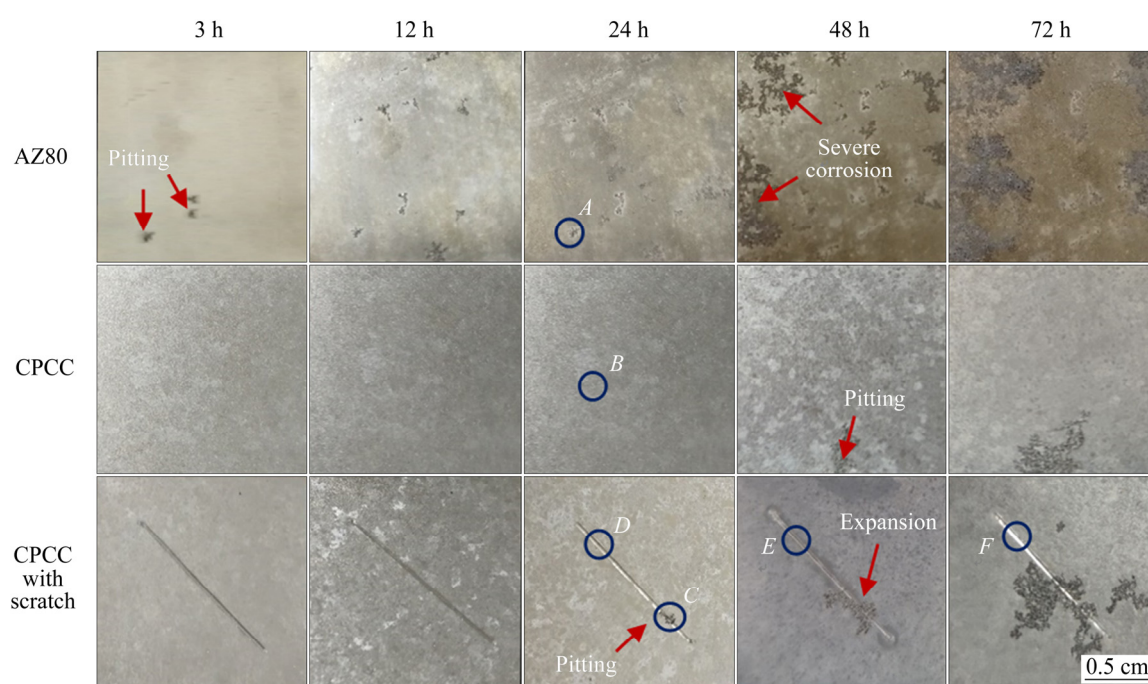


Fig. 6 Morphologies of AZ80, CPCC and CPCC with scratch immersed in 3.5 wt.% NaCl solution for different time

surface of AZ80 underwent severe corrosion. Pitting corrosion initiated on CPCC after 48 h immersion, indicating an enhanced corrosion resistance. In the case of CPCC with scratch, pitting corrosion firstly occurred after being immersed for 24 h. In addition, as the immersion time increased, the corrosion expanded from the scratch to the surroundings.

In order to further analyze the corrosion characteristics, the microstructures of the specimens immersed for 24 h were selected for comparison. The microstructures observed at zones *A*, *B*, *C* and *D* in Fig. 6 are shown in Fig. 7. AZ80 had obvious corrosion (Fig. 7(a)) and the CPCC had local spalling (Fig. 7(b)). In the case of the scratched coating, there was some pitting corrosion in some scratch areas, as shown in Fig. 7(c). However, the appearance at Zone *D* (Fig. 7(d)) indicated that corrosion was not remarkable in other scratched areas.

3.2.3 Hydrogen evolution

To further explore the corrosion resistance of CPCC and the effect of the scratch on the corrosion resistance of CPCC, hydrogen evolution

experiments were carried out in the 3.5 wt.% NaCl solution. The results (Fig. 8) show that the hydrogen evolution rate of AZ80 is the fastest. After phosphating, the hydrogen evolution rate of the alloy decreased and the corrosion resistance was improved. The hydrogen evolution rate of CPCC with scratch was higher than that of CPCC, but still lower than that of AZ80, which is consistent with the results of electrochemical testing.

3.3 Corrosion mechanism

The results of electrochemical test and immersion test showed that CPCC had a protective effect on the AZ80 magnesium alloy substrate, and the scratch decreased the corrosion resistance of CPCC. In order to explore the mechanism of the scratch on the corrosion behaviour of CPCC, the SVET and SEM of CPCC with scratch immersed in NaCl solution for different time were studied.

3.3.1 Local electrochemical analysis

SVET could exhibit the local electrochemical behaviour, including the distribution and magnitude of the cathodic and anodic activity on the corroded area [46,47]. Thus, SVET was used to characterize

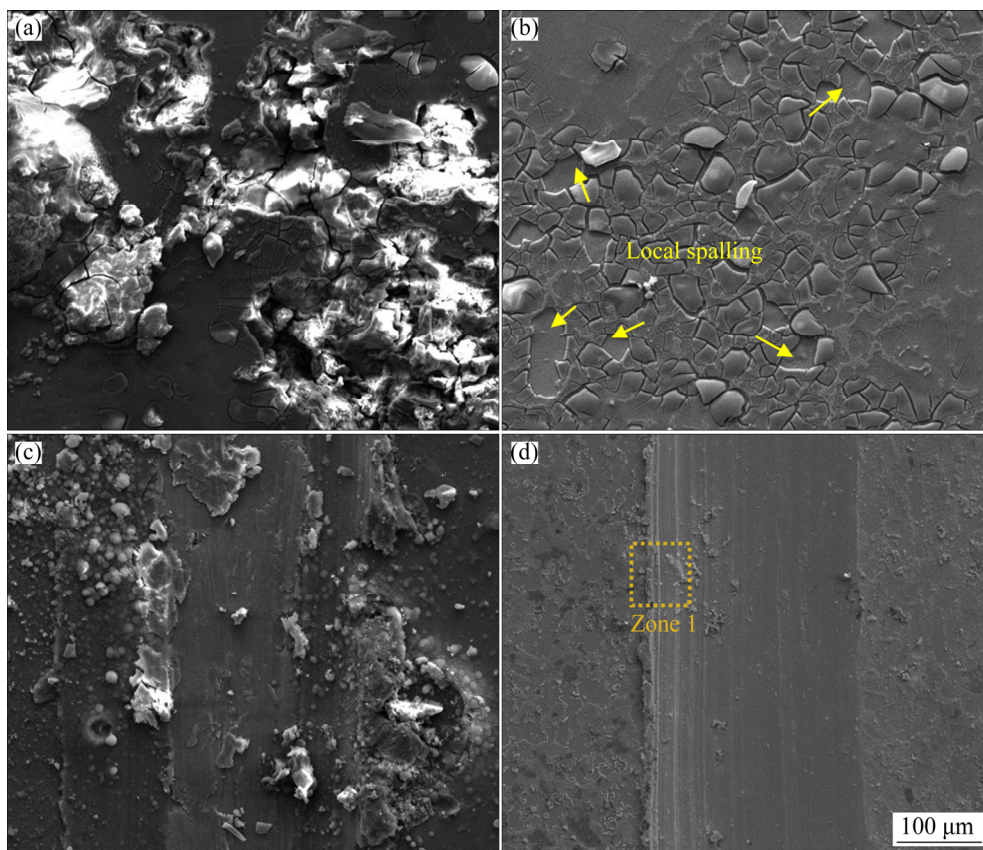


Fig. 7 SEM images of specimens immersed in 3.5 wt.% NaCl solution for 24 h at different zones in Fig. 6: (a) AZ80 (Zone *A*); (b) CPCC (Zone *B*); (c) CPCC with scratch (Zone *C*); (d) CPCC with scratch (Zone *D*)

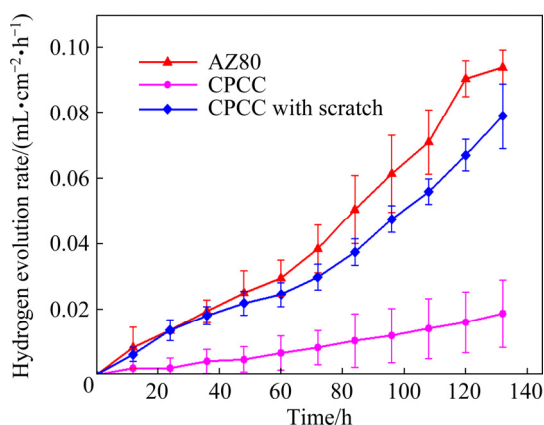


Fig. 8 Hydrogen evolution rate of AZ80, CPCC and CPCC with scratch immersed in 3.5 wt.% NaCl solution

the corrosion behaviour of CPCC with scratch for different immersion time. The optical microstructure of the scratched coating before the test and the SVET maps after 15 min, 1 h, 3 h and 6 h immersion in corrosive solution are presented in Fig. 9. The SVET map after 15 min immersion (Fig. 9(b)) shows that the potential of the scratch area (as pointed by the black arrows) was lower than that of non-scratch area, indicating that the anodic region occurred initially at the scratch area.

The strong corrosion in the scratch area occurred because of the direct contact between the exposed magnesium alloy substrate at the scratch and the NaCl corrosive solution. When the immersion time increased to 1 h (Fig. 9(c)), there was small potential difference between the scratch area and the non-scratch area. This indicated that there was no obvious local corrosion in the scratch area. It is assumed that the accumulated film of corrosion products caused the reduction of the corrosion rate [40]. With the further increase of the immersion time to 3 and 6 h, affected by the edge effect, no obvious corrosion was found in the scratch areas, and the whole test areas exhibited mainly global corrosion. Hence, it was concluded from the SVET that the scratch mainly affected the initial stage of corrosion by inducing local corrosion.

3.3.2 Corrosion morphology evolution

To further understand the corrosion process of the coating with scratch, SEM images of the specimens immersed for 24, 48 and 72 h were characterized in detail.

The image of CPCC with scratch immersed in 3.5 wt.% NaCl solution for 24 h at Zone 1 in Fig. 7 is shown in Fig. 10(a). Figures 10(b)–(d) are local

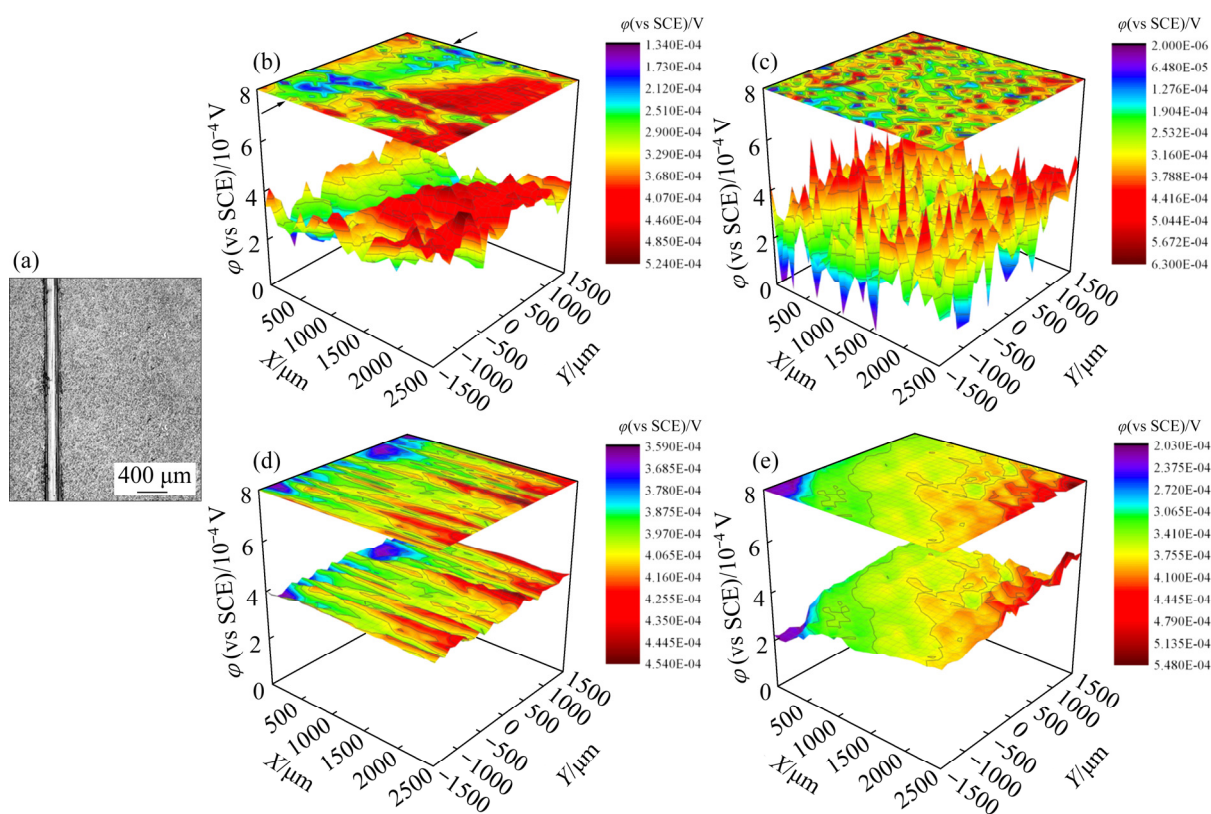
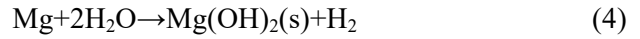


Fig. 9 Optical image of CPCC with scratch before immersion in 3.5 wt.% NaCl (a), and SVET maps after immersion for 15 min (b), 1 h (c), 3 h (d) and 6 h (e)

enlarged images of Fig. 10(a), which represent the area of the coating, the AZ80 substrate area and the bonding area between the coating and the substrate, respectively. After immersion in NaCl solution for 24 h, a small number of particles and flocs were formed on the CPCC (Fig. 10(b)). The evenly distributed flower-like clusters and some granular products were formed on the substrate (Fig. 10(c)). At the same time, the obvious lamellar corrosion products were formed in the scratch (Fig. 10(d)). The result of EDS (Fig. 10(e)) showed that the lamellar corrosion products were mainly composed of Mg, O and Al. Generally, the corrosion reaction of magnesium alloy in NaCl solution is usually

formed by electrochemical reaction with water to form H_2 and $Mg(OH)_2$ [31]:



It was observed that corrosion occurred initially at the scratch. Such phenomenon may be due to the potential difference between the AZ80 substrate and the coating, resulting in galvanic corrosion in the NaCl solution [48,49]. Furthermore, the corrosion firstly occurred at the junction between the scratch and the coating rather than in the scratch groove. We speculate that this may be

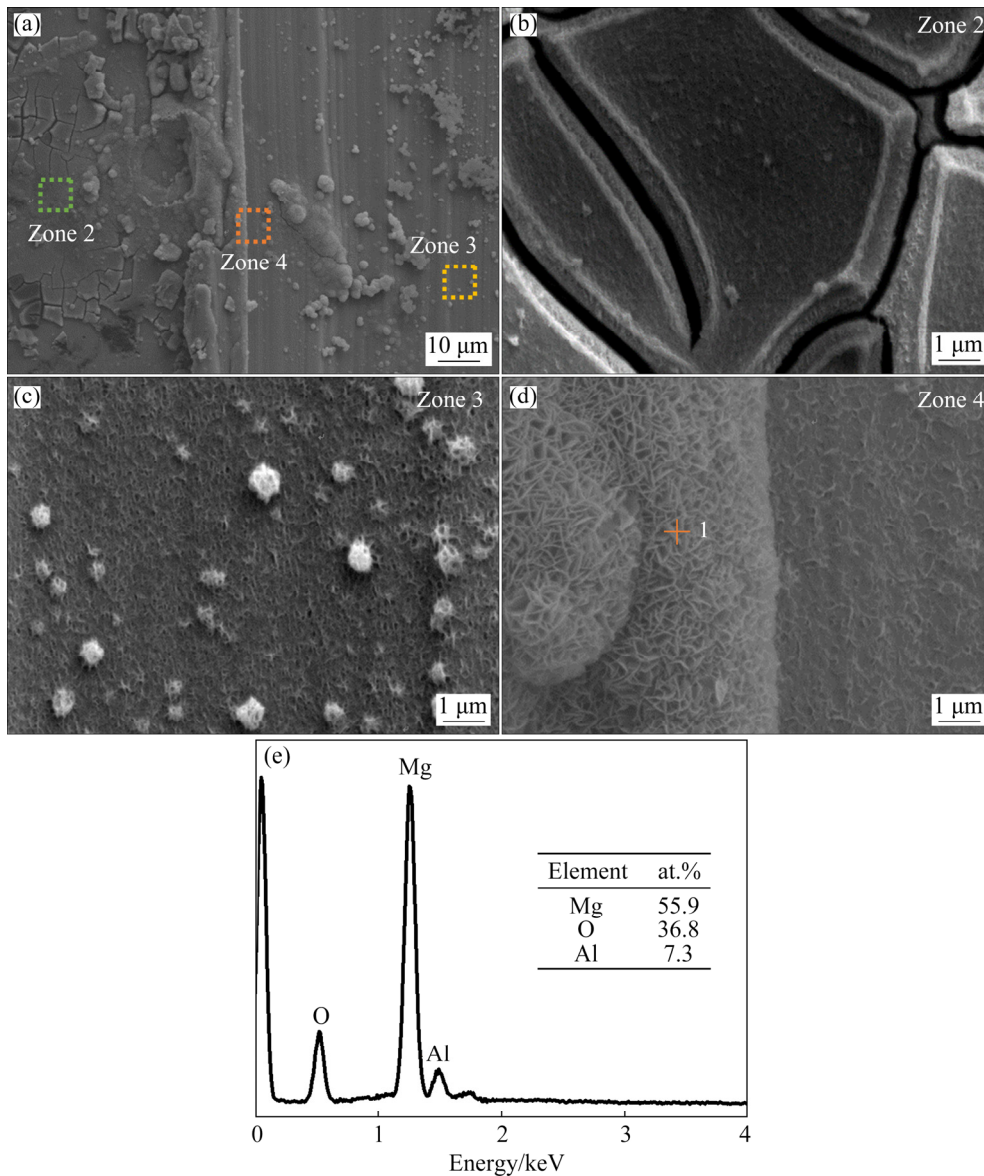


Fig. 10 SEM images of CPCC with scratch immersed in 3.5 wt.% NaCl solution for 24 h: (a) Overall morphology (Zone 1 in Fig. 7(d)); (b) Zone 2 for CPCC; (c) Zone 3 for substrate; (d) Zone 4 for junction of coating and substrate; (e) EDS spectrum of Point 1 in (d)

due to the compressive stress in the groove during the scratch [50]. According to the work from UMENO et al [51], the compressive stress would inhibit the diffusion of atoms along grain boundaries, while the tensile stress would promote the diffusion. SIBENER et al [52] further reported that the tensile stress can accelerate the electrochemical reactivity on the alloy surface, while compressive stress can inhibit it. Therefore, the externally applied compressive stress in the groove during scratch inhibited the corrosion. In contrast, the tensile stress at the junction between the scratch and the coating aggravated the corrosion.

In order to further clarify the influence of the scratch on the corrosion behaviour of the coating, the surface morphologies of the coatings with and

without scratch were observed after immersion for 48 and 72 h, as shown in Fig. 11. As for the scratched specimens, after immersion in NaCl solution for 48 h, the accumulation of corrosion products occurred on the AZ80 substrate, compared with immersion for 24 h (Fig. 10(c)), and the CPCC was cracked and spalled (Fig. 11(a)). In addition, the lamellar corrosion products $Mg(OH)_2$ were found on the CPCC (Fig. 11(b)). This is because chloride ions in the solution are more likely to reach the magnesium alloy matrix through the cracks and then cause corrosion [53]. After immersion in NaCl solution for 72 h, most of the CPCC detached (Fig. 11(d)). In addition, there were corrosion products and large cracks on the remained coating (Fig. 11(e)), indicating that the specimen exhibited severe corrosion even for the coating. For the

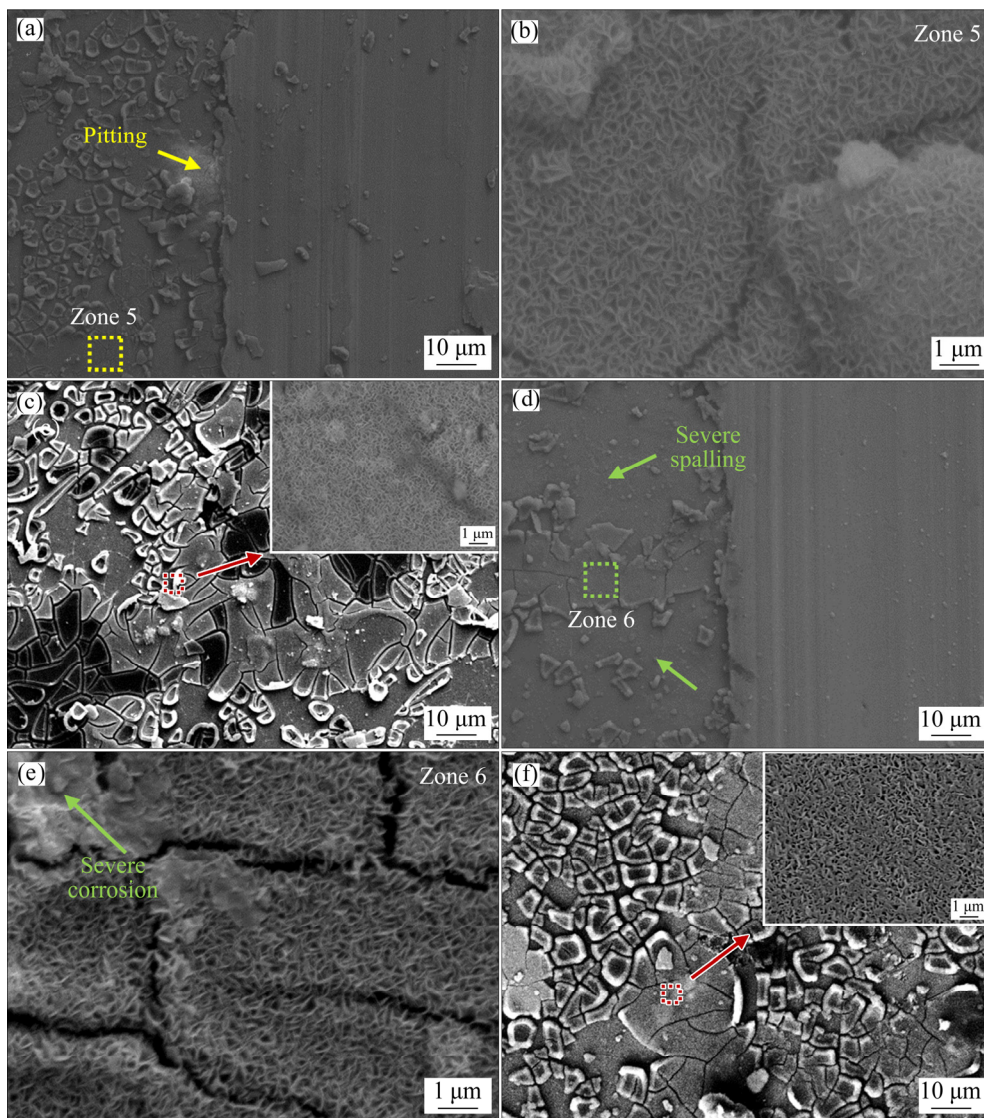


Fig. 11 SEM images of CPCC with scratch immersed in 3.5 wt.% NaCl solution for 48 h (a, b) (Zone E in Fig. 6) and 72 h (d, e) (Zone F in Fig. 6), and coating without damage immersed in 3.5 wt.% NaCl solution for 48 h (c) and 72 h (f)

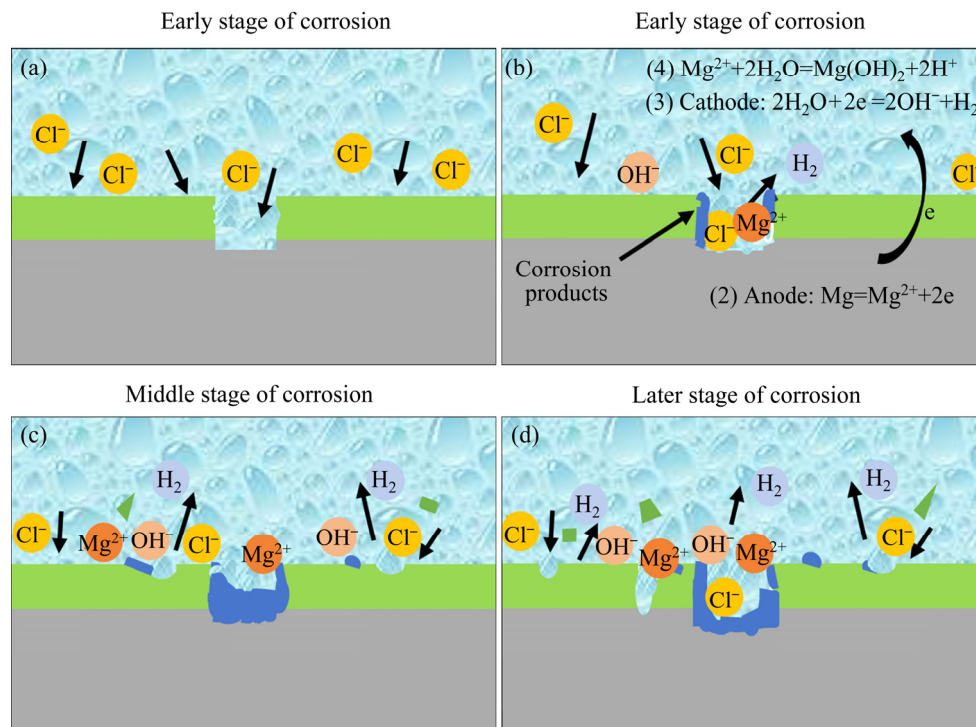


Fig. 12 Schematic showing corrosion process and mechanism of CPCC with scratch in 3.5 wt.% NaCl solution at various immersion time

specimens without scratch, the chemical conversion coating peeled off locally, and fine layered corrosion products were found on the coating after immersion for 48 h, as shown in Fig. 11(c). When the immersion time increased to 72 h, the coatings seriously cracked and partially peeled off. The flocculent corrosion products formed on the surface of coating (Fig. 11(f)). Obviously, the corrosion degrees of the specimens without damage were lower than those of the scratched specimens. Therefore, the scratch had a great influence on the corrosion behavior of the specimens which would accelerate the corrosion of the specimens because of the opened corrosion channel.

3.3.3 Corrosion model

Based on the clarification of corrosion mechanism of AZ80, CPCC and CPCC with scratch, a schematic model was established, as shown in Fig. 12. In the early corrosion stage, the scratched coating was immersed in the 3.5 wt.% NaCl solution rich in corrosive ions (Fig. 12(a)). The corrosion firstly occurred at the junction of the scratch and the CPCC (Fig. 12(b)). This is because a corrosion channel was built resulting from the scratch to the CPCC, which was associated with the NaCl solution directly arriving at the AZ80

magnesium alloy substrate through the scratch. The Cl^- reached the Mg alloy substrate and induced the chemical reactions (Reactions (2)–(4)). Furthermore, the tensile stress from the scratching process accelerated the local corrosion at the junction of the scratch and the CPCC. In the middle corrosion stage, the brittle and hard coating began to detach from the AZ80 substrate (Fig. 12(c)). A few local corrosion pits also occurred on the CPCC. At the same time, the generated corrosion products mainly deposited on the scratch area. As the immersion time further increased, a large corrosion channel was formed (Fig. 12(d)). The CPCC was also significantly corroded. As a result, the corrosion resistance of the coating began to decline.

4 Conclusions

(1) A calcium phosphate conversion coating was prepared successfully on AZ80 magnesium alloy with a thickness of about 800 nm. The main phase of the coating was the dicalcium phosphate dihydrate.

(2) The scratch had an important effect on the corrosion resistance of the calcium phosphate conversion coated AZ80 because of the damage to

the coating. The scratch with a width of around 200 μm , a length of about 12 mm on the coating deteriorated the corrosion resistance from a current density of (4 ± 1) to (39 ± 1) $\mu\text{A}/\text{cm}^2$.

(3) SVET showed that the corrosion occurred first in the scratch area. Furthermore, the local corrosion initially occurred at the junction of scratch and the coating due to the opened corrosion channel and tensile stress. The scratch could also accelerate the cracking and peeling of the coating around it. With increasing immersion time, the corrosion expanded from the scratch to the coating area.

Acknowledgments

This work was financially supported by the National Natural Science Foundation of China (Nos. 52071036, 51701027), the Fundamental Research Funds for the Central Universities, China (Nos. 2020CDJQY-A002, 2021CDJCGJ009), and the National Key Research and Development Program of China (Nos. 2016YFB0301100, 2016YFB0101700).

References

- [1] DING Xing-xing, WU Liang, ZHENG Zhi-cheng, MA Yan-long, ATRENS A, CHEN Xiao-bo, XIE Zhi-hui, SUN De-en, PAN Fu-sheng. Fabrication and characterization of an actively protective Mg–Al LDHs/ Al_2O_3 composite coating on magnesium alloy AZ31 [J]. *Applied Surface Science*, 2019, 487: 558–568.
- [2] ZHANG Gen, WU Liang, TANG Ai-tao, MA Yan-long, SONG Guang-ling, ZHENG Da-jiang, JIANG Bin, ATRENS A, PAN Fu-sheng. Active corrosion protection by a smart coating based on a MgAl-layered double hydroxide on a cerium-modified plasma electrolytic oxidation coating on Mg alloy AZ31 [J]. *Corrosion Science*, 2018, 139: 370–382.
- [3] SONG Jiang-feng, SHE Jia, CHEN Dao-lun, PAN Fu-sheng. Latest research advances on magnesium and magnesium alloys worldwide [J]. *Journal of Magnesium and Alloys*, 2020, 8: 1–41.
- [4] GUO Yang-yang, QUAN Gao-feng, JIANG Ying-long, REN Ling-bao, FAN Ling-ling, PAN Hou-hong. Formability, microstructure evolution and mechanical properties of wire arc additively manufactured AZ80M magnesium alloy using gas tungsten arc welding [J]. *Journal of Magnesium and Alloys*, 2020, 8: 192–201.
- [5] LIU Qiang, SONG Jiang-feng, PAN Fu-sheng, SHE Jia, ZHANG Shuo, PENG Peng. The edge crack, texture evolution, and mechanical properties of Mg–1Al–1Sn–Mn alloy sheets prepared using on-line heating rolling [J]. *Metals*, 2018, 8: 1–14.
- [6] KUMAR D, PHANDEN R K, THAKUR L. A review on environment friendly and lightweight magnesium-based metal matrix composites and alloys [J]. *Materials Today: Proceedings*, 2021, 38: 359–364.
- [7] VOIDT T, LIPP K, MELZ T. Fatigue strength assessment for components and subsystems of a lightweight, space saving city car with electric drive [J]. *Procedia Structural Integrity*, 2019, 19: 4–11.
- [8] GRAF M, ULLMANN M, KAWALLA R. Influence of initial state on forgeability and microstructure development of magnesium alloys [J]. *Procedia Engineering*, 2014, 81: 546–551.
- [9] MAURYA R, SIDDIQUI A R, BALANI K. An environment-friendly phosphate chemical conversion coating on novel Mg–9Li–7Al–1Sn and Mg–9Li–5Al–3Sn–1Zn alloys with remarkable corrosion protection [J]. *Applied Surface Science*, 2018, 443: 429–440.
- [10] LI Ling-jie, LI Xia, CHEN Jin-long, LIU Lei, LEI Jing-lei, LI Nian-bing, LIU Gao, PAN Fu-sheng. One-step spraying method to construct superhydrophobic magnesium surface with extraordinary robustness and multi-functions [J]. *Journal of Magnesium and Alloys*, 2020, 9: 668–675.
- [11] SONG Y W, SHAN D Y, HAN E H. High corrosion resistance of electroless composite plating coatings on AZ91D magnesium alloys [J]. *Electrochimica Acta*, 2008, 53: 2135–2143.
- [12] ZHAO Yu-chao, TANG Jian-cheng, YE Nan, ZHOU Wei-wei, WEI Chao-long, LIU Ding-jun. Influence of additives and concentration of WC nanoparticles on properties of WC–Cu composite prepared by electroplating [J]. *Transactions of Nonferrous Metals Society of China*, 2020, 30: 1594–1604.
- [13] WANG Ying, GU Zheng-peng, LIU Jia, JIANG Jian, YUAN Ning-yi, PU Ji-bin, DING Jian-ning. An organic/inorganic composite multi-layer coating to improve the corrosion resistance of AZ31B Mg alloy [J]. *Surface and Coatings Technology*, 2019, 360: 276–284.
- [14] ALIOFKHAZRAEI M, TOORANI M, MAHDAVIAN M, NADERI R. Effective PEO/silane pretreatment of epoxy coating applied on AZ31B Mg alloy for corrosion protection [J]. *Corrosion Science*, 2020, 169: 1–15.
- [15] FAZAL B R, PHUONG N V, MOON S. Cerium- and phosphate-based sealing treatments of PEO coated AZ31 Mg alloy [J]. *Surface and Coatings Technology*, 2017, 309: 86–95.
- [16] AN Ling-yun, MA Ying, YUAN Xiao-xu, WANG Sheng, WANG Zhan-ying. Effects of electrical parameters and their interactions on plasma electrolytic oxidation coatings on aluminum substrates [J]. *Transactions of Nonferrous Metals Society of China*, 2020, 30: 883–895.
- [17] ZHANG Zhao-qi, WANG Li, ZENG Mei-qi, ZENG Rong-chang, LIN Cun-guo, WANG Zhen-lin, CHEN Dong-chu, ZHANG Qiang. Corrosion resistance and superhydrophobicity of one-step polypropylene coating on anodized AZ31 Mg alloy [J]. *Journal of Magnesium and Alloys*, 2020, 9(4): 1443–1457.
- [18] NIU Li-yuan, CHANG Shiuan-Ho, TONG Xian, LI Guang-yu, SHI Zi-mu. Analysis of characteristics of vanadate conversion coating on the surface of magnesium alloy [J]. *Journal of Alloys and Compounds*, 2014, 617: 214–218.

- [19] JAYAN P S, JANA P, MANDAL S, BISWASA K. Hot corrosion behaviour of rare-earth magnesium hexaaluminate based thermal barrier coatings under molten sulphate-vanadate salts [J]. *Surface and Coatings Technology*, 2017, 322: 108–119.
- [20] MA Yi-bin, LI Ning, LI De-yu, ZHANG Mi-lin, HUANG Xiao-mei. Characteristics and corrosion studies of vanadate conversion coating formed on Mg–14wt%Li–1wt%Al–0.1wt%Ce alloy [J]. *Applied Surface Science*, 2012, 261: 59–67.
- [21] XU Peng-fei, LU Xiang-yu, CHENG Hong-xia, FENG Xing-guo, ZHAO Zuo-peng, DING Yan-xu, SHEN Ya-lin, SHI Xing-ling. Investigation of the surface modification of magnesium particles with stannate on the corrosion resistance of a Mg-rich epoxy coating on AZ91D magnesium alloy [J]. *Progress in Organic Coatings*, 2019, 135: 591–600.
- [22] SU Ying-chao, GUO Yun-ting, HUANG Zi-long, ZHANG Zhi-hui, LI Guang-yu, LIAN Jian-she, REN Lu-quan. Preparation and corrosion behaviors of calcium phosphate conversion coating on magnesium alloy [J]. *Surface and Coatings Technology*, 2016, 307: 99–108.
- [23] CARVALHO S M, BRAGA J O, SILVA L M C, SOARES R B, LINS V F C, MAZZER E M, HOUMARD M, FIGUEIREDO R B, NUNES E H M. Fabrication and characterization of dicalcium phosphate coatings deposited on magnesium substrates by a chemical conversion route [J]. *Surface and Coatings Technology*, 2020, 386: 1–11.
- [24] ATRENS A, SONG Guang-ling, SUOHN D. An hydrogen evolution method for the estimation of the corrosion rate of magnesium alloys [J]. *Magnesium Technology*, 2001, 255–262.
- [25] FAN Xiao-li, LI Chang-yang, WANG Yu-bo, HUO Yuan-fang, LI Shuo-qi, ZENG Rong-chang. Corrosion resistance of an amino acid-bioinspired calcium phosphate coating on magnesium alloy AZ31 [J]. *Journal of Materials Science and Technology*, 2020, 49: 224–235.
- [26] SHI Zhi-ming, ATRENS A. An innovative specimen configuration for the study of Mg corrosion [J]. *Corrosion Science*, 2011, 53: 226–246.
- [27] LIU Yang, LIU Xiao, ZHANG Ze-chuan, FRRELL N, CHEN Da-fu, ZHENG Yu-feng. Comparative, real-time in situ monitoring of galvanic corrosion in Mg–Mg₂Ca and Mg–MgZn₂ couples in Hank's solution [J]. *Corrosion Science*, 2019, 161: 1–9.
- [28] YIN Zheng, HE Ren-hua, CHEN Yang, YIN Zhou, YAN Kun, WANG Kun, YAN Hong, SONG Hong-gun, YIN Cheng-xin, GUAN Hong-yu, LUO Chao, HU Zhi, LUC C. Effects of surface micro-galvanic corrosion and corrosive film on the corrosion resistance of AZ91–xNd alloys [J]. *Applied Surface Science*, 2021, 536: 147761–147771.
- [29] TEUR I F, ARDELEAN H, MARCUS P. Corrosion protection of magnesium alloys by cerium, zirconium and niobium-based conversion coatings [J]. *Corrosion Science*, 2008, 50: 1907–1918.
- [30] CHU Y R, LEE Y L, LI W C, LIN C S. Effect of permanganate concentration on the formation and properties of phosphate/permanganate conversion coating on AZ31 magnesium alloy [J]. *Corrosion Science*, 2013, 70: 74–81.
- [31] GUPTA M, PHUONG N V, MOON S. Enhanced corrosion performance of magnesium phosphate conversion coating on AZ31 magnesium alloy [J]. *Transactions of Nonferrous Metals Society of China*, 2017, 27: 1087–1095.
- [32] ZHOU Peng, YU Bao-xing, HOU Yao-jun, DUAN Guo-qing, YANG Li-xin, ZHANG Bo, ZHANG Tao, WANG Fu-hui. Revisiting the cracking of chemical conversion coating on magnesium alloys [J]. *Corrosion Science*, 2021, 178: 1–13.
- [33] MA Xiao-dong, FENG Xi, GUO Jie, CAO Hui-qin, SUO Xue-yue, SUN Hong-wen, ZHENG Mei-hua. Catalytic oxidation of 1,2-dichlorobenzene over Ca-doped FeO_x hollow microspheres [J]. *Applied Catalysis B: Environmental*, 2014, 147: 666–676.
- [34] LATHA B S, BHARATH G, ALSHARAEH E H, PRAKASH P, PONPANDIAN N. Enhanced hydroxyapatite nanorods formation on graphene oxide nanocomposite as a potential candidate for protein adsorption, pH controlled release and an effective drug delivery platform for cancer therapy [J]. *The Royal Society of Chemistry*, 2017, 9: 240–252.
- [35] KHALIL A J, FATHYUNES L, MOOSAVIFAR M. Development of graphene oxide/calcium phosphate coating by pulse electrodeposition on anodized titanium: Biocorrosion and mechanical behavior [J]. *Journal of the Mechanical Behavior of Biomedical Materials*, 2019, 90: 575–586.
- [36] ZAI Wei, SU Ying-chao, MAN H C, LIAN Jian-she, LI Guang-yu. Effect of pH value and preparation temperature on the formation of magnesium phosphate conversion coatings on AZ31 magnesium alloy [J]. *Applied Surface Science*, 2019, 492: 314–327.
- [37] PU S, SOLIMAN H, ZHANG W, MAKHLOUF A S, WAN G. Deposition of anti-corrosion hybrid film of hexamethylene diaminetetrakis (methylene phosphonic acid)/hydroxyapatite on biodegradable Mg: Influence of deposition procedures [J]. *Surface and Coatings Technology*, 2020, 402: 126242–126250.
- [38] CHEN Jun-feng, LIN Wen-xin, LIANG Shi-yan, ZOU Lin-chi, WANG Chen, WANG Bin-shu, YAN Mu-fu, CUI Xi-ping. Effect of alloy cations on corrosion resistance of LDH/MAO coating on magnesium alloy [J]. *Applied Surface Science*, 2019, 463: 535–544.
- [39] ZHANG Gen, TANG Ai-tao, WU Liang, ZHANG Ze-yu, LIAO Hong-xin, LONG Ying, LI Ling-jie, ATRENS A, PAN Fu-sheng. In-situ grown super- or hydrophobic Mg–Al layered double hydroxides films on the anodized magnesium alloy to improve corrosion properties [J]. *Surface & Coatings Technology*, 2019, 366: 238–247.
- [40] WANG Sheng-nan, GU Yan-hong, GENG Yin-liang, LIANG Jian, ZHAO Jie, KANG Ju. Investigating local corrosion behavior and mechanism of MAO coated 7075 aluminum alloy [J]. *Journal of Alloys and Compounds*, 2020, 826: 153976–153989.
- [41] BIRBILIS N, KING A D, SCULLY J R. Accurate electrochemical measurement of magnesium corrosion rates: A combined impedance, mass-loss and hydrogen collection study [J]. *Electrochimica Acta*, 2014, 121: 394–406.
- [42] SU Ying-chao, GUO Yun-ting, GU Rui, ZHANG Zhi-hui, LI Guang-yu, LIAN Jian-she, REN Lu-quan. Enhanced corrosion resistance and biocompatibility of biodegradable

- magnesium alloy modified by calcium phosphate/collagen coating [J]. *Surface & Coatings Technology*, 2020, 401: 1–12.
- [43] ALIOFKHAZRAEI M, NABAVI H F, ROUHAGHDAM A S. Electrical characteristics and discharge properties of hybrid plasma electrolytic oxidation on titanium [J]. *Journal of Alloys and Compounds*, 2017, 728: 464–475.
- [44] LI Ling-yu, CUI Lan-yue, LIU Bin, ZENG Rong-chang, CHEN Xiao-bo, LI Shuo-qi, WANG Zhen-lin, HAN En-hou. Corrosion resistance of glucose-induced hydrothermal calcium phosphate coating on pure magnesium [J]. *Applied Surface Science*, 2019, 465: 1066–1077.
- [45] WU Peng-peng, ZHANG Zhong-zhong, XU Fang-jun, DENG Kun-kun, NIE Kai-bo, GAO Rui. Effect of duty cycle on preparation and corrosion behavior of electrodeposited calcium phosphate coatings on AZ91 [J]. *Applied Surface Science*, 2017, 426: 418–426.
- [46] BASTOS A C, TEDIM J, KALLIP S, ZHELUDKEVICH M L, FERREIRA M G S. Corrosion protection of AA2024-T3 by LDH conversion films: Analysis of SVET results [J]. *Electrochimica Acta*, 2016, 210: 215–224.
- [47] GELLING V J, YAN M, HINDERLITER B R, BATTOCCHI D, TALLMAN D E, BIERWAGEN G P. SVET method for characterizing anti-corrosion performance of metal-rich coatings [J]. *Corrosion Science*, 2010, 52: 2636–2642.
- [48] BAI Li-jing, KOU Gang, ZHAO Kai, CHEN Gui-tao, YAN Fu-xue. Effect of in-situ micro-arc oxidation coating on the galvanic corrosion of AZ31Mg coupled to aluminum alloys [J]. *Journal of Alloys and Compounds*, 2019, 775: 1077–1085.
- [49] FENG Zhen-liang, SONG Guang-Ling, XU Yu-qing, ZHENG Da-jiang, CHEN Xiao-dong. Micro-galvanic corrosion during formation of epoxy coating [J]. *Progress in Organic Coatings*, 2020, 147: 105799–105809.
- [50] FRANKEL G S, LIU Xiao-dong. Effects of compressive stress on localized corrosion in AA2024-T3 [J]. *Corrosion Science*, 2006, 48: 3309–3329.
- [51] UMENO Y, KITAMUKA T, OHTANI K. Molecular dynamics study on grain boundary diffusion in aluminum under hydrostatic stress [J]. *JSME International Journal Series A*, 1998, 41: 147–152.
- [52] SIBENER S J, HAHM J. Stress-modified electrochemical reactivity of metallic surfaces: Atomic force microscopy imaging studies of nickel and alloyed aluminum [J]. *Applied Surface Science*, 2000, 161: 375–384.
- [53] YIN Mo-yang, LI Zhou, XIAO Zhu, PANG Yong, LI Ya-ping, SHEN Zi-yan. Corrosion behavior of Cu–Al–Mn–Zn–Zr shape memory alloy in NaCl solution [J]. *Transactions of Nonferrous Metals Society of China*, 2021, 31: 1012–1022.

划痕对 AZ80 镁合金上磷酸钙转化涂层耐腐蚀性能的影响

贾雪娇¹, 宋江凤^{1,2}, 屈小荣³, 曹福勇⁴, 蒋斌^{1,2}, Andrej ATRENS⁵, 潘复生^{1,2}

1. 重庆大学 机械传动国家重点实验室, 重庆 400044;

2. 重庆大学 国家镁合金材料工程技术研究中心, 重庆 400044;

3. 青海盐湖工业股份有限公司, 青海 816000;

4. 厦门大学 材料学院 海洋材料腐蚀防护研究中心, 厦门 361005;

5. School of Mechanical and Mining Engineering, The University of Queensland, Brisbane Qld 4072, Australia

摘要: 通过电化学测试、扫描振动电极技术、浸泡实验和析氢实验分析 AZ80 合金、磷酸钙转化涂层以及含划痕涂层的耐腐蚀性能, 进而研究划痕对 AZ80 镁合金上磷酸钙转化膜腐蚀行为的影响。结果表明, AZ80 合金经涂层处理后腐蚀性能提高, 其腐蚀电流密度由 $(85\pm 4) \mu\text{A}/\text{cm}^2$ 降低为 $(4\pm 1) \mu\text{A}/\text{cm}^2$ 。当涂层被破坏后, 其对基体的保护能力下降。涂层上一条长约 12 mm 的划痕可使其腐蚀电流密度增加到 $(39\pm 1) \mu\text{A}/\text{cm}^2$ 。此外, 样品上的划痕区域最先开始腐蚀, 进一步观察发现, 腐蚀发生于划痕与涂层的交界处。由此, 提出含划痕涂层的显微腐蚀机理。

关键词: 镁合金; AZ80 合金; 划痕; 转化膜; 腐蚀性能; 扫描振动电极技术(SVET)

(Edited by Xiang-qun LI)